

# 000 001 002 003 004 005 006 007 008 009 010 011 012 013 014 015 016 017 018 019 020 021 022 023 024 025 026 027 028 029 030 031 032 033 034 035 036 037 038 039 040 041 042 043 044 045 046 047 048 049 050 051 052 053 DECODING LARGE LANGUAGE DIFFUSION MODELS WITH FORESEEING MOVEMENT

Anonymous authors

Paper under double-blind review

## ABSTRACT

Large Language Diffusion Models (LLDMs) benefit from a flexible decoding mechanism that enables parallelized inference and controllable generations over autoregressive models. Yet such flexibility introduces a critical challenge: inference performance becomes highly sensitive to the decoding order of tokens. Existing heuristic methods, however, focus mainly on local effects while overlooking long-term impacts. To address this limitation, we propose the Foreseeing Decoding Method (FDM), a novel approach that integrates both local and global considerations to unlock the full potential, employing a search-based strategy to enable effective optimization in discrete spaces. Furthermore, by analyzing the consistency of chosen tokens in the full decoding process, we develop a variant, FDM with Acceleration (FDM-A), which restricts deep exploration to critical steps identified as the exploration and balance circumferences. Extensive experiments across diverse benchmarks and model architectures validate the scalability of FDM and demonstrate the superior efficiency-performance trade-off achieved by FDM-A. Our work might potentially provide a principled step toward more powerful decoding methods for LLDMs.

## 1 INTRODUCTION

In recent years, diffusion models (Ho et al., 2020; Rombach et al., 2022a) have emerged as a promising competitor in natural language modeling (Nie et al., 2025; DeepMind, 2025), challenging the dominance of auto-regressive generation (Jaech et al., 2024; Guo et al., 2025; Team et al., 2025). Instead of generating tokens sequentially from left to right and token by token, Large Language Diffusion Models (LLDMs) can generate multiple tokens in parallel, making it highly efficient at the inference stage (Li et al., 2025; Khanna et al., 2025). In addition, owing to pipelines of processing denoising and the bidirectional modeling, LLDMs can outperform the auto-regressive models in broad aspects such as reverse reasoning (Berglund et al., 2024), controllable generation (Xiong et al., 2025; Li et al., 2022), or multi-modal reasoning (Li et al., 2025).

However, high flexibility is a double-edged sword, as it can lead to performance degradation if sampling paths are chosen inappropriately, attributing to the convergence issues (Li & Cai, 2025) and the non-convexity of the optimization goal (Kim et al., 2025; Peng et al., 2025; Ben-Hamu et al., 2025). For example, as shown in Table 1, compared to decoding with a random order, decoding answers with the order of the largest marginal probability yields an improvement on the ARC benchmark (Clark et al., 2018) from 79.06% to 82.55%, underscoring its critical importance. To address this issue, previous works have mainly developed strategies from a heuristic perspective. For example, pioneer works (Nie et al., 2025; Zheng et al., 2024) propose to decode by enlarging the predicted probability. Follow-up works argue that probability margins (Kim et al., 2025) and the entropy of the predicted distribution (Ben-Hamu et al., 2025) are better substitutes, considering that LLDMs may be confused when the probabilities of the topmost tokens at the given position are near. However, though effective, previous heuristic approaches decode tokens with local information at each step, overlooking the long-term impacts underlying the full decoding paths without leveraging the full potentiality of LLDMs at the inference stage.

Table 1: The performances of LLaDA with various decoding orders on the ARC (Clark et al., 2018) benchmark.

	Random	Margin	FDM-A
Accuracy ( $\uparrow$ )	79.06	82.55	<b>86.30</b>
Tokens/Seconds ( $\uparrow$ )	12.01	10.85	<b>38.20</b>

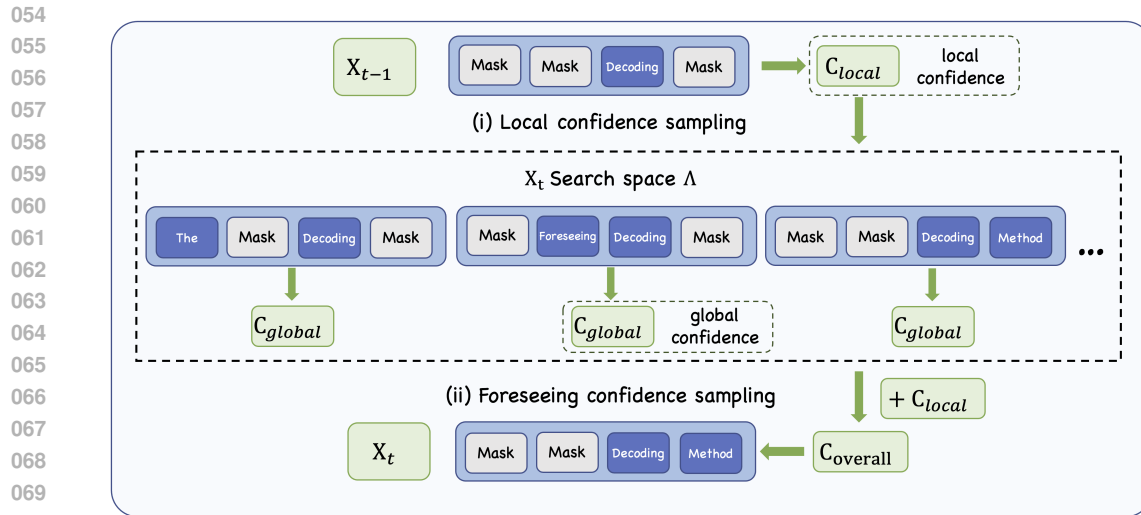


Figure 1: The pipeline of FDM. We first **compress** the search space into a small set  $\Lambda$  by filtering out candidates of lower local confidence *i.e.*  $C_{local}$ . In the final, we incorporate both local and global confidence to decide the ultimate choice at step  $t$ .

Therefore, in this paper, with further analyzing the decoding formulation of LLDMs, we find that it can be divided into two components. The first one is termed as **local confidence** in Figure 1 (i), reflecting the uncertainty of models in predicting a given token and widely adopted by the heuristic methods. The other is the **global confidence**, capturing the future impact in decoding a specific token. It is not directly accessible and typically ignored by prior methods. However, we demonstrate that the training goal of LLDMs provides a good approximation. By further combining both of them into considerations, we propose **Foreseeing Decoding Method** (FDM), illustrated in Figure 1. To ensure the computation is affordable in reality, the decoding process of FDM is divided into two stages: We firstly rank the candidate tokens with **their local confidence**. In the second competition, the overall criterion of both local and global confidence is adopted to decide the final tokens chosen for decoding. We not only theoretically prove FDM will achieve lower errors compared to heuristic methods but also perform experiments across multiple benchmarks to illustrate that the benefit of it can further improve by enlarging the search space. It demonstrates FDM will serve as a test-time **scaling** (Snell et al., 2024; Bi et al., 2024) method specifically designed for LLDMs.

Furthermore, by calculating the consistency ratio of FDM and the simple confidence-based decoding, we find that a global view is not always necessary at every step, especially when the context is sufficient for reliable decisions. Motivated by this observation, we propose an accelerated version of FDM (FDM-A). It will perform an adaptive exploration from the probability feedback, switching to FDM only when all candidates have low confidence or borderline scenarios. As shown in Table 1, FDM-A can not only accelerate the decoding process with over  $3\times$  speed-up but also obtain notable performances. In summary, our contributions are listed as follows:

- We propose the **Foreseeing Decoding Method** (FDM) to **schedule the decoding orders of LLDMs**. Unlike heuristic approaches, it takes both the local and global confidence as the criterion for decision, guaranteeing a lower divergence with the natural distribution.
- Motivated by the agreement ratio in decoding, we further accelerate FDM with an adaptive strategy (FDM-A). It adaptively performs exploration when the context is rare and parallel decodes tokens if models have enough context for complete generation.
- The experiments across multiple benchmarks and variants of LLDMs are performed, manifesting the scalability of FDM and the outstanding performance of FDM-A in balancing efficiency and performance.

108 **2 RELATED WORK**

110 **Large Language Diffusion Models (LLDMs).** As one of the most successful types of generative  
 111 models, the popularity of diffusion models has been well-recognized in the vision domain (Ho  
 112 et al., 2020; Peebles & Xie, 2023; Rombach et al., 2022b). At the training stage, the model predicts  
 113 the noises added to the natural inputs. Then, at the test time, by utilizing the model to denoise  
 114 step by step, diffusion models recover the original data through iterative refinement. Inspired by  
 115 their great success, early investigations such as D3PMs (Austin et al., 2021), DiffuSeq (Gong  
 116 et al., 2023) have demonstrated the potential of the diffusion pipeline in language tasks. However,  
 117 limited to the small scales, their performances are considerably inferior to those of their auto-  
 118 regressive competitors. Recently, LLaDA (Nie et al., 2025; Zhu et al., 2025) scales the model  
 119 parameters to billions, **considered as one of the most representative works in Large Language**  
 120 **Diffusion Models (LLDMs).** To save the computational costs, other architectures like Dream (Ye et al.,  
 121 2025), DiffuGPT (Gong et al., 2024), and Dream-Coder (Xie et al., 2025) perform continual training  
 122 on the pretrained weights of the auto-regressive counterparts. Built upon the outstanding performances  
 123 in the language capacity, large language diffusion models have also been applied to multi-modal  
 124 applications such as biomedical understanding (Dong et al., 2025), chart understanding (You et al.,  
 125 2025), and mathematical reasoning (Yang et al., 2025). But in this paper, we propose FDM to improve  
 126 the performance of LLDMs at the inference stage.

127 **Decoding Order of LLDMs.** With the rapid development of LLDMs, their shortcomings are also  
 128 disclosed. One of the most prominent ones is the vital significance of the decoding orders (Kim et al.,  
 129 2025). This is because when the context is limited, models will fail to accurately predict all tokens.  
 130 In other words, the uncertainty of predictions can be measured with the output probability. This  
 131 motivates the heuristic-based approaches, including **decoding with the largest probability value** (Nie  
 132 et al., 2025; Zheng et al., 2024), with the largest margin probability (Kim et al., 2025), and with  
 133 the least entropy of distribution (Ben-Hamu et al., 2025). Although heuristic methods improve the  
 134 performance of LLDMs a lot **compared to decoding with the random order**, they make decisions  
 135 based on local confidence, ignoring the sequential consequence to other tokens. This limitation may  
 136 bring errors to the generated sequences. **Thus, in this paper, we propose FDM and FDM-A, which**  
 137 **incorporate the global confidence to depict the future cascading effect in the decoding process.** .

138 **Acceleration of LLDMs.** Although LLDMs map to the complete answer at each step, they will  
 139 suffer a quality-efficiency trade-off with a varying decoding step (Feng et al., 2025; Nie et al., 2025).  
 140 In addition, to achieve the bidirectional attentions, the attention maps of LLDMs are not causal,  
 141 requiring model-agnostic methods like KV-Cache for adaptations. Therefore, in a series of works (Wu  
 142 et al., 2025; Hu et al., 2025; Ma et al., 2025), they propose their own approximation acceleration for  
 143 reusing the Key-Value, largely accelerating the inference speed. More related to our work, Hong  
 144 et al. (2025) and Ben-Hamu et al. (2025) both propose samplers for dynamic decoding in LLDMs.  
 145 But Hong et al. (2025) purely focus on the **parallel decoding** for acceleration and Ben-Hamu et al.  
 146 (2025) propose WINO for revoking suspicious error tokens. While in our paper, we propose FDM-A  
 147 to balance the explorations and accelerations in decoding, **achieving a better trade-off**.

148 **3 PRELIMINARIES**

149 Unlike auto-regressive models that generate answers in a sequential way, LLDMs define a Markov  
 150 chain that revises the answer step-by-step with a denoised process. Given the user query  $\mathbf{q}$  and the  
 151 vocabulary space  $M = \{1, 2, \dots, m\}$ , the generation of final answer  $\mathbf{x}_T$  with length  $L$  under the data  
 152 distribution  $p_{data}$  can be formulated as:

$$154 \quad \mathbf{x}_T = \arg \max_{\mathbf{x}_T} p_{data}(\mathbf{x}_{0:T} | \mathbf{q}) = \arg \max_{\mathbf{x}_T} p(\mathbf{x}_0) \prod_{\alpha=1}^{T-1} p_{data}(\mathbf{x}_\alpha | \mathbf{q}, \mathbf{x}_{0:\alpha-1}), \quad (1)$$

155 where  $p(\mathbf{x}_0)$  is sampled from an initial noise distribution which is independent to  $\mathbf{q}$ .  $\mathbf{x}_\alpha$  is a partially  
 156 masked sequence at the  $\alpha$  step. **To analyze the influence of the intermediate variable  $\mathbf{x}_t$ , we can**  
 157 **regroup the terms associated with step  $t$  as:**

$$158 \quad \mathbf{x}_T = \arg \max_{\mathbf{x}_T} p_{data}(\mathbf{x}_{t+1:T} | \mathbf{q}, \mathbf{x}_{0:t}) p_{data}(\mathbf{x}_t | \mathbf{q}, \mathbf{x}_{t-1}) \prod_{\alpha=1}^{t-1} p_{data}(\mathbf{x}_\alpha | \mathbf{q}, \mathbf{x}_{0:\alpha-1}). \quad (2)$$

162 Although the above equation shows that  $\mathbf{x}_t$  can impact future variables from  $\mathbf{x}_{t+1}$  to  $\mathbf{x}_T$ , heuristic  
 163 decoding methods commonly simplify the procedure by focusing solely with the local partition:  
 164

$$\pi_H(\mathbf{x}_t | \mathbf{x}_{t-1}) : \mathbf{x}_t = \arg \max_{\mathbf{x}_t} p_\theta(\mathbf{x}_t | \mathbf{q}, \mathbf{x}_{t-1}), \quad (3)$$

165 where  $\theta$  is a parameterized neural network introduced by LLDMs to model the natural distribution.  
 166 According to (Nie et al., 2025), the optimization target of LLDMs can be given as:

$$\mathbb{E}_{\mathbf{x}_T \sim p_{data}, t \in [0, T]} \frac{1}{n} \sum_{j=1}^n \mathbf{1}[\mathbf{x}_t^{(j)} = \text{Mask}] \odot \log p_\theta(\mathbf{q}, \mathbf{x}_t^{(j)})[\mathbf{x}_T], \quad (4)$$

167 where  $\odot$  is the Hadamard product and  $[\mathbf{x}_T]$  represents the probability value of the tokens in  $\mathbf{x}_T$ . With  
 168 a well-trained model, LLDMs learn to approximate the conditional log-probability of future tokens in  
 169  $\mathbf{x}_m$  given the current masked state,  $\mathbf{x}_t$  ( $m > t$ ) and the user query  $\mathbf{q}$ . Specifically,

$$\log p_\theta(\mathbf{x}_m | \mathbf{x}_t, \mathbf{q}) = \mathbf{1}[\mathbf{x}_m \neq \text{Mask} \& \& \mathbf{x}_t = \text{Mask}] \odot \log p_\theta(\mathbf{q}, \mathbf{x}_t)[\mathbf{x}_m], \quad (5)$$

170 which follows from the fact that the model predicts the token distribution for any masked position  
 171 independently.

## 172 4 METHODOLOGY

### 173 4.1 THE FORESEEING DECODING METHOD

174 Although Equation 3 establishes a simple formulation in decoding  $\mathbf{x}_t$ , ignoring the contribution of  $\mathbf{x}_t$   
 175 in  $p_{data}(\mathbf{x}_{t+1:T} | \mathbf{q}, \mathbf{x}_{0:t})$  might mislead the decoding process, leading the unexpected errors in the  
 176 generative response. Therefore, differing from previous works, our proposed Foreseeing Decoding  
 177 Method (FDM) aims to decode tokens that achieve the largest value across the overall formulation  
 178 and its decoding strategy can be given as:

$$\pi_F(\mathbf{x}_t | \mathbf{q}, \mathbf{x}_{t-1}) : \mathbf{x}_t = \arg \max_{\mathbf{x}_t} p_\theta(\mathbf{x}_T | \mathbf{q}, \mathbf{x}_t) p_\theta(\mathbf{x}_t | \mathbf{q}, \mathbf{x}_{t-1}). \quad (6)$$

179 Here we replace  $p_{data}(\mathbf{x}_{t+1:T} | \mathbf{q}, \mathbf{x}_{0:t})$  with  $p_\theta(\mathbf{x}_T | \mathbf{q}, \mathbf{x}_t)$  owing to the property of the Markov Chain  
 180 and the modeling of LLDMs. From the theoretical perspective, we also prove that under  $\pi_F$ , the  
 181 generative distribution achieves lower KL divergence with the natural distribution  $p_{data}$  than that of  
 182  $\pi_H$ :

183 **Theorem 1.** Let  $\Delta_{total} \triangleq \sum_{t=1}^T \mathbb{E}_{p_{data}(\mathbf{x}_{t-1})} [\mathcal{I}_{p_{data}}(\mathbf{x}_t; \mathbf{x}_T | \mathbf{x}_{t-1})]$ , where  $\mathcal{I}_{p_{data}}(\mathbf{x}_t; \mathbf{x}_T | \mathbf{x}_{t-1})$  is  
 184 the conditional mutual information under  $q$ . Then

$$D_{KL}(p_{data}(\mathbf{x}), p_{\pi_F}) = D_{KL}(p_{data}(\mathbf{x}), p_{\pi_H}) - \Delta_{total}. \quad (7)$$

185 For the complete proof, please refer to Appendix B for more details. Due to the fact that mutual  
 186 information is non-negative, we derive that the generative distribution under  $\pi_F$  has lower KL  
 187 divergence with the natural distribution  $p_{data}$  than  $\pi_H$ . By further applying the log transformation  
 188 to Equation 6, we can obtain,

$$\mathbf{x}_t = \arg \max_{\mathbf{x}_t} \{\log p_\theta(\mathbf{x}_T | \mathbf{q}, \mathbf{x}_t) + \log p_\theta(\mathbf{x}_t | \mathbf{q}, \mathbf{x}_{t-1})\}. \quad (8)$$

189 With deeper analysis, we find the first term captures how decoding a specific token influences the  
 190 future (the **global** confidence,  $C_{global}$ ), while the second term reflects the model's confidence in  
 191 decoding it at step  $t$  (the **local** confidence,  $C_{local}$ ). According to Equation 5,  $C_{global}$  can be estimated  
 192 by:

$$C_{global} = \log p_\theta(\mathbf{x}_T | \mathbf{x}_t, \mathbf{q}) = \mathbf{1}[\mathbf{x}_T \neq \text{Mask} \& \& \mathbf{x}_t = \text{Mask}] \odot \log p_\theta(\mathbf{q}, \mathbf{x}_t)[\mathbf{x}_T]. \quad (9)$$

193 Regarding  $\mathbf{x}_T$  is a full response without any mask,  $\mathbf{x}_T \neq \text{Mask}$  can be omitted since it holds for  
 194 every position. In addition, instead of greedily decoding  $\mathbf{x}_T$  from the model output to calculate  
 195  $C_{global}$ . We compute the expectation over the entire model output distribution:

$$C_{global} = \mathbf{1}[\mathbf{x}_t = \text{Mask}] \odot \mathbb{E}_{p_\theta} \log p_\theta(\mathbf{q}, \mathbf{x}_t). \quad (10)$$

---

216 **Algorithm 1** Foreseeing Decoding Method (FDM)

---

217 **Input:** User query  $\mathbf{q}$ , the partially decoded sequence  $\mathbf{x}_{t-1}$ , pruning threshold  $\gamma$ , width  $K$ , well-  
 218 trained models  $\theta$ , the number of tokens for decoding  $n$ .  
 219 // Get the candidate tokens of the undecoded positions.  
 220 Candidate =  $[\mathbf{1}[\mathbf{x}_{t-1} = \text{Mask}] \odot \arg \max p_\theta(\mathbf{q}, \mathbf{x}_{t-1})]$   
 221 **for**  $x_t$  in Candidate **do**  
 222   **if**  $p_\theta(\mathbf{q}, \mathbf{x}_{t-1})[x_t] \leq \gamma$  **then**  
 223     Delete  $x_t$  from Candidate.  
 224   **end if**  
 225 **end for**  
 226 Priority Queue  $\{\mathbf{x}_t\}$  of the priority  $C_{local}$  by foreseeing decoding  $n$  tokens from Candidate.  
 227 // Narrow the search space with the width  $K$ .  
 228  $\Lambda = \text{Top-K}(\{\mathbf{x}_t\})$   
 229 **if**  $\Lambda = \emptyset$  **then**  
 230    $\mathbf{x}_t = \arg \max C_{local}(\mathbf{x}_t)$   
 231 **else**  
 232   Calculate  $C_{global}(\mathbf{x}_t)$  for each  $\mathbf{x}_t$  in  $\Lambda$   
 233    $\mathbf{x}_t = \arg \max_{\mathbf{x}_t \in \Lambda} \{C_{local}(\mathbf{x}_t) + C_{global}(\mathbf{x}_t)\}$   
 234 **end if**  
 235 **Output:** The decoded answer  $\mathbf{x}_t$  at step  $t$

---

236  
 237 In addition, with Equation 5, we can formulate  $C_{local}$  with:  
 238

$$C_{local} = \mathbf{1}[\mathbf{x}_t \neq \text{Mask} \& \& \mathbf{x}_{t-1} = \text{Mask}] \odot \log p_\theta(\mathbf{q}, \mathbf{x}_{t-1})[\mathbf{x}_t]. \quad (11)$$

239 Similar to the denotation in Equation 5, here  $[\mathbf{x}_t]$  means the predicted probability of each token in  $\mathbf{x}_t$ .  
 240 After combining both equations, we have:  
 241

$$\begin{aligned} 242 \mathbf{x}_t &= \arg \max_{\mathbf{x}_t} \{ \mathbf{1}[\mathbf{x}_t = \text{Mask}] \odot \mathbb{E}_{p_\theta} \log p_\theta(\mathbf{q}, \mathbf{x}_t) \\ 243 &\quad + \mathbf{1}[\mathbf{x}_t \neq \text{Mask} \& \& \mathbf{x}_{t-1} = \text{Mask}] \odot \log p_\theta(\mathbf{q}, \mathbf{x}_{t-1})[\mathbf{x}_t] \}. \end{aligned} \quad (12)$$

244 Note that in this equation,  $p_\theta(\mathbf{q}, \mathbf{x}_{t-1})$  is independent of  $\mathbf{x}_t$ , which can be accurately calculated by  
 245 querying the model  $\theta$  with the acquired sequence  $\mathbf{x}_{t-1}$  and user prompt  $\mathbf{q}$ . In contrast, the  $p_\theta(\mathbf{q}, \mathbf{x}_t)$   
 246 takes the discrete variable  $\mathbf{x}_t$  as a part of the input. It means every evaluation involves a single  
 247 forward pass. To resolve this problem, we introduce the hyperparameter  $K$  to compress the search  
 248 space for efficiency. In detail, we first obtain the set of candidate tokens with the prediction of  $\theta$  on  
 249 the masked position:  
 250

$$251 \text{Candidate} = \{\mathbf{1}[\mathbf{x}_{t-1} = \text{Mask}] \odot \arg \max p_\theta(\mathbf{q}, \mathbf{x}_{t-1})\} \quad (13)$$

252 Furthermore, to avoid being trapped in the local optima, we also incorporate a dynamic pruning  
 253 strategy that retains only candidate tokens whose confidence exceeds the predefined threshold  $\gamma$ .  
 254 Then,  $C_{local}$  is introduced as the metric to rank each possibility of  $\mathbf{x}_t$  and we only keep the Top- $K$   
 255 candidates for further decision. Thus, the search space  $\Lambda$  can be defined as:  
 256

$$257 \Lambda = \{\mathbf{x}_t | \mathbf{x}_t \in \text{Top-K}(\{\mathbf{x}_t\}), \mathbf{1}[\mathbf{x}_t \neq \text{Mask} \& \& \mathbf{x}_{t-1} = \text{Mask}] \odot p_\theta(\mathbf{q}, \mathbf{x}_{t-1})[\mathbf{x}_t] > \gamma\}. \quad (14)$$

258 Defined on  $\Lambda$ , our proposed Foreseeing Decoding Method (FDM) is formulated as follows,  
 259

$$\begin{aligned} 260 \mathbf{x}_t &= \begin{cases} \arg \max_{\mathbf{x}_t \in \{\mathbf{x}_t\}} C_{local}(\mathbf{x}_t) & \text{if } \Lambda = \emptyset \\ 261 \arg \max_{\mathbf{x}_t \in \Lambda} \{C_{local}(\mathbf{x}_t) + C_{global}(\mathbf{x}_t)\} & \text{if } \Lambda \neq \emptyset \end{cases} \end{aligned} \quad (15)$$

262 We also summarize the whole decoding process of FDM at the  $t$  step in Algorithm 1.

## 263 4.2 ACCELERATION WITH THE FORESEEING DECODING METHOD

264 Based on the analysis in Section 4.1, in this section, we further investigate a variant, *i.e.*, FDM-A  
 265 to better balance the decoding speed and performance. In Figure 2, we calculate the consistency

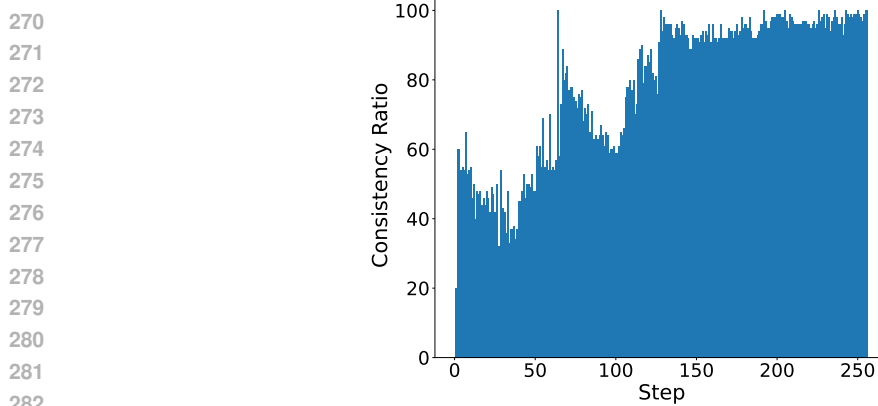


Figure 2: The consistency ratio of selecting the next decoding token using  $C_{local}$  alone versus both  $C_{local}$  and  $C_{global}$ . The decisions of both strategies are made based on the same  $\mathbf{x}_{t-1}$  in each step. Peak points are observed on the steps of 64 and 128 because we follow the [proposed](#) semi-autoregressive pipeline in (Nie et al., 2025) with the block size 64.

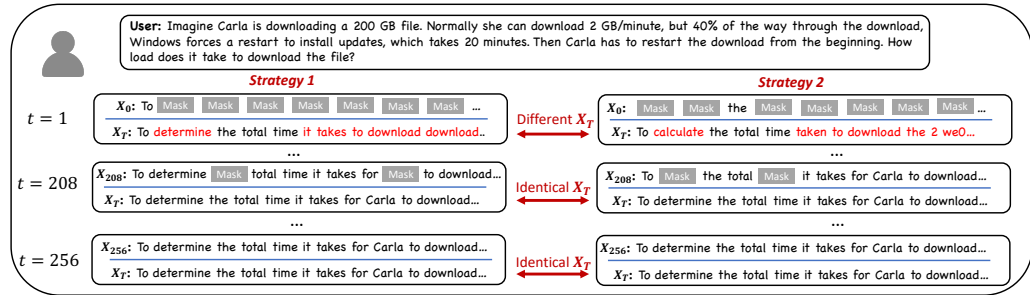


Figure 3: The effect of different decoding [strategy](#) to  $\mathbf{x}_T$  at the step  $t$  given the identical  $\mathbf{x}_{t-1}$ . The influence gradually decreases as  $t$  increases from 0 to  $T$ .

ratio in token selection with local confidence only ([heuristic decoding](#)) versus both local and global confidence. We average the results over the first 100 examples in the GSM8K (Cobbe et al., 2021) test set. The experiments are performed on LLaDA (Nie et al., 2025), with  $\gamma = 0.6$  and  $K = 2$ .

In the early stages of decoding, due to limited context, the overlap between the two decoding strategies is relatively low, at approximately 50%. However, as decoding progresses, the degree of overlap gradually increases and finally exceeds 90%. It consists of the [empirical](#) observation in Figure 3, the final decoding sequence ( $\mathbf{X}_T$ ) is largely shaped when  $t$  is small. But when  $t$  is approaching  $T$ , most unmasked tokens have been determined by the adequate contexts, indicating the marginal impact of decoding orders. This evidence demonstrates that more exploration from the global confidence is needed at the beginning, while at the final stage, we only need to adopt the local confidence to accelerate the decoding.

Motivated by this observation, we divide the entire process into three stages: **the exploration, balance and acceleration phases** by incorporating two hyperparameters, *i.e.*  $\eta_1$  and  $\eta_2$ . Firstly, in the exploration phase, if there are no tokens whose [prediction probability](#) exceeds  $\eta_1$ , we will perform exploration with FDM. We denote it with  $FDM_1(\mathbf{x}_{t-1}, \mathbf{q}, n)$ , initialized with the  $K_1$ .  $n$  is the number of tokens decoded in this step and we set it to 1 for reliability. Thus  $\mathbf{x}_t$  can be given as:

$$FDM_1(\mathbf{x}_{t-1}, \mathbf{q}, n = 1, \gamma = \gamma_1). \quad (16)$$

In the balance phase, we focus on the intermediate states of the decoding process. We combine the exploration and acceleration to achieve a good trade-off. Specifically, we refer to the tokens whose probability lies between  $\eta_1$  and  $\eta_2$  as the “Borderline Tokens” and those that have the [prediction probability](#) greater than  $\eta_1$  as the “Qualified Tokens”. By applying FDM, we weigh options within a collection comprising both sets. The number of decoding tokens,  $n$  is set as  $NUM([\mathbf{x}_{t-1} = \text{Mask}]p_\theta(\mathbf{q}, \mathbf{x}_{t-1}) > \eta_1)$  for acceleration and  $NUM(\cdot)$  is a function that counts the

324

**Algorithm 2** Acceleration with FDM (FDM-A)

325

326

327

328

329

330

331

332

333

334

335

336

337

338

339

340

341

342

343

344

345

346

347

348

349

350

351

352

353

354

355

356

357

358

359

360

361

362

363

364

365

366

367

368

369

370

371

372

373

374

375

376

377

**Input:** User query  $\mathbf{q}$ , fully masked sequence  $\mathbf{x}_0$ , pruning threshold  $\gamma_1$ , searching width  $K_1$ , stage division coefficients  $\eta_1$  and  $\eta_2$ , upper bound for the decoding number  $N$ , well-trained models  $\theta$ .

Initialize FDM with  $K = K_1$  and get  $\text{FDM}_1$ .

Initialize FDM with  $K = 1$  and get  $\text{FDM}_2$ .

$t = 1$

**while** Mask not in  $\mathbf{x}_t$  **do**

**if**  $\text{NUM}([\mathbf{x}_{t-1} = \text{Mask}]p_\theta(\mathbf{q}, \mathbf{x}_{t-1}) > \eta_1) = 0$  **then**

$\mathbf{x}_t = \text{FDM}_1(\mathbf{x}_{t-1}, \mathbf{q}, n = 1, \gamma = \gamma_1)$

**else if**  $\text{NUM}([\mathbf{x}_{t-1} = \text{Mask}]p_\theta(\mathbf{q}, \mathbf{x}_{t-1}) > \eta_1) \geq N$  **then**

$\mathbf{x}_t = \text{FDM}_2(\mathbf{x}_{t-1}, \mathbf{q}, n = N, \gamma = 1.0)$

**else if**  $\text{NUM}(\eta_2 < [\mathbf{x}_{t-1} = \text{Mask}]p_\theta(\mathbf{q}, \mathbf{x}_{t-1}) \leq \eta_1) = 0$  **then**

$\mathbf{x}_t = \text{FDM}_2(\mathbf{x}_{t-1}, \mathbf{q}, n = \text{NUM}([\mathbf{x}_{t-1} = \text{Mask}]p_\theta(\mathbf{q}, \mathbf{x}_{t-1}) > \eta_1), \gamma = 1.0)$

**else**

$\mathbf{x}_t = \text{FDM}_1(\mathbf{x}_{t-1}, \mathbf{q}, n = \text{NUM}([\mathbf{x}_{t-1} = \text{Mask}]p_\theta(\mathbf{q}, \mathbf{x}_{t-1}) > \eta_1), \gamma = \eta_2)$

**end if**

$t = t + 1$

**end while**

**Output:** Generated answer  $\mathbf{x}_t$ .

number of tokens that meet the given condition. The formulation of decoding  $\mathbf{x}_t$  is:

$$\text{FDM}_1(\mathbf{x}_{t-1}, \mathbf{q}, n = \text{NUM}([\mathbf{x}_{t-1} = \text{Mask}]p_\theta(\mathbf{q}, \mathbf{x}_{t-1}) > \eta_1), \gamma = \eta_2), \quad (17)$$

As shown in Figure 3, different decoding methods perform almost the same at the tail, [indicating the convergence in decoding](#). At this time, we shift the mode to the acceleration phase. The tokens are decoded with the local confidence [only](#) to achieve the fastest speed. The decoding function can be regarded as a special case of FDM. By initializing it with  $K = 1$ , we represent it by  $\text{FDM}_2(\mathbf{x}_{t-1}, \mathbf{q}, n)$  and  $\mathbf{x}_t$  can be decoded with:

$$\text{FDM}_2(\mathbf{x}_{t-1}, \mathbf{q}, n = \min(\text{NUM}([\mathbf{x}_{t-1} = \text{Mask}]p_\theta(\mathbf{q}, \mathbf{x}_{t-1}) > \eta_1), N), \gamma = 1.0). \quad (18)$$

$N$  is the upper bound for clipping the decoding number of tokens.

We term this acceleration decoding pipeline as FDM-A. The algorithm of it is summarized in [Algorithm 2](#).

## 5 EXPERIMENT

### 5.1 MAIN RESULTS

**Benchmark and Metrics:** To demonstrate the effectiveness of FDM and FDM-A, we conduct experiments on four prevailing benchmark datasets: GSM8K ([Cobbe et al., 2021](#)), HumanEval ([Chen et al., 2021](#)), Countdown ([Zhao et al., 2025](#)) and ARC ([Clark et al., 2018](#)). They reflect the capabilities of LLDMs in four aspects, including math issue solutions, code generation, logic reasoning, and common sense knowledge. Meanwhile, for the convenience of evaluation, following ([Hong et al., 2025](#)), we add a system prompt before each input item. The details of them in each dataset are summarized in [Appendix C](#). All evaluations are performed under the zero-shot condition to ensure the fairness. For performances, we take accuracy as the metric, manifesting the percentage of [queries](#), that could be properly [answered](#) by LLDMs. For efficiency, we choose Tokens Per Second (TPS) [as the metric](#). It is defined as the number of tokens generated in [one](#) second.

**Baselines and models:** We compare FDM with three heuristic-based decoding methods: decoding with the highest probability (Probability) ([Nie et al., 2025](#); [Zheng et al., 2024](#)), with the highest marginal probability (Margin) ([Kim et al., 2025](#)) and with the lowest entropy (Entropy) ([Ben-Hamu et al., 2025](#)). For FDM-A, since it tries to balance between efficiency and performance, we also compare it with the newest dynamic decoding methods for LLDMs in recent months: EB (Entropy Bounded Sampler) ([Ben-Hamu et al., 2025](#)) and WINO ([Hong et al., 2025](#)). To ensure

378  
 379 Table 2: Comparison (%) of FDM with the heuristic decoding strategies across four benchmarks. With  
 380 the scale up of the wide  $K$ , we see that accuracy increases with the decrease of TPS, demonstrating  
 381 that FDM serves as an inference-time scaling method.

382 Benchmark	383 Method	384 LLaDA		385 LLaDA-1.5		386 MMaDA-MixCoT		387 LLaDA-MoE	
		388 Accuracy	389 TPS	390 Accuracy	391 TPS	392 Accuracy	393 TPS	394 Accuracy	395 TPS
396 GSM8K	Probability ( $T=256$ )	81.20	11.51	82.10	11.89	56.18	11.26	76.50	4.13
	Margin ( $T=256$ )	80.14	11.23	82.18	11.39	56.18	10.97	76.80	4.04
	Entropy ( $T=256$ )	80.12	10.79	81.93	10.94	54.91	10.51	76.80	3.84
	FDM ( $K=2$ )	82.03	8.28	82.49	8.29	57.54	8.18	77.48	3.80
	FDM ( $K=3$ )	82.18	5.86	82.64	5.84	57.68	5.71	77.63	3.78
	FDM ( $K=4$ )	82.34	4.61	83.02	4.69	57.92	4.61	78.32	3.60
397 HumanEval	Probability ( $T=256$ )	42.68	9.24	42.68	9.20	12.80	8.91	56.71	3.81
	Margin ( $T=256$ )	43.29	8.76	42.68	8.83	12.80	8.65	58.54	3.81
	Entropy ( $T=256$ )	40.24	8.67	42.68	8.67	11.59	8.28	59.15	3.56
	FDM ( $K=2$ )	43.29	6.55	43.29	6.66	12.80	6.32	59.76	3.72
	FDM ( $K=3$ )	44.51	4.63	43.29	4.51	12.80	4.60	59.76	3.67
	FDM ( $K=4$ )	45.73	3.66	44.51	3.71	13.40	3.64	60.37	3.47
398 Countdown	Probability ( $T=256$ )	18.75	11.19	16.02	11.20	4.69	11.15	40.62	4.15
	Margin ( $T=256$ )	19.14	10.89	20.31	10.92	14.61	10.84	40.23	4.03
	Entropy ( $T=256$ )	18.44	10.39	20.31	10.39	7.03	10.31	38.67	3.95
	FDM ( $K=2$ )	19.14	8.21	20.70	8.62	14.45	8.13	40.62	3.73
	FDM ( $K=3$ )	21.09	6.11	21.88	6.48	16.40	6.10	46.10	3.71
	FDM ( $K=4$ )	25.00	5.28	23.43	5.25	17.58	4.97	46.88	3.70
400 ARC	Probability ( $T=256$ )	80.96	10.96	87.06	10.98	58.26	10.94	76.19	4.01
	Margin ( $T=256$ )	82.55	10.85	87.44	10.82	56.37	10.62	75.85	4.01
	Entropy ( $T=256$ )	78.13	10.43	87.38	10.38	58.33	10.18	71.84	3.98
	FDM ( $K=2$ )	86.00	7.72	88.18	7.71	59.43	7.68	82.89	3.85
	FDM ( $K=3$ )	86.46	5.58	88.45	5.59	59.61	5.58	83.45	3.73
	FDM ( $K=4$ )	86.68	4.58	88.59	4.56	59.76	4.37	83.51	3.64

401 the generalability of the observations, we cover four variants of LLDMs: LLaDA-8B-Instruct (Nie  
 402 et al., 2025), LLaDA-1.5 (Zhu et al., 2025), LLaDA-MoE-7B-Instruct (inclusionAI, 2025) and  
 403 MMaDA-8B-MixCoT (Yang et al., 2025).

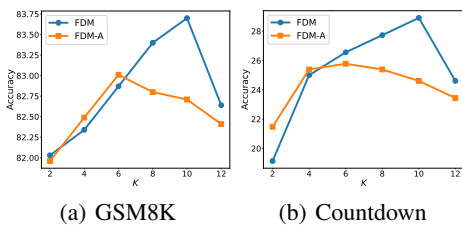
404 **Hyperparameters:** Consistent with the observation in (Nie et al., 2025), we observe that the semi-  
 405 autoregressive pipeline is vital to maintain a satisfying performance for the instruct models of LLDMs.  
 406 Thus we applying it for decoding with the generation length 256, block size 64. The step number  
 407  $T$  is fixed to 256 and 128, respectively for the heuristic decoding methods when comparing them  
 408 with FDM or FDM-A. The threshold in EB is set as 0.5.  $\tau_1$  and  $\tau_2$  in WINO are configured as 0.7  
 409 and 0.9. For our method,  $\gamma$  for the dynamic pruning is 0.6 for FDM and 0.5 for FDM-A considering  
 410 explorations are less performed in FDM-A. For the threshold for stage division, we set  $\eta_1$  to 0.8 and  
 411  $\eta_2$  to 0.7. We gradually increase the width of FDM from 2 to 4 and set the default width of FDM-A  
 412 as 2. All experiments are performed on a single NVIDIA A100 80G GPU.

413 **Results:** Firstly, in Table 2, we observe that FDM surpasses baseline methods across all models and  
 414 benchmarks, demonstrating the significance of exploration with the global confidence. For example,  
 415 on the LLaDA model and ARC benchmarks, the highest score of the heuristic methods is 82.55%,  
 416 and FDM with the search width 2 is 86.00%. In addition, scaling up the width  $K$  can further enhance  
 417 its performance, demonstrating its role in serving as an inference-time scaling technique. An example  
 418 is that on the LLaDA-MoE and GSM8K benchmark, the accuracy improves from 77.48% to 78.32%  
 419 when the width rises from 2 to 4. It is worth noting that this improvement is notable since we do not  
 420 need a verifier or optimize the parameters. It demonstrates that FDM well fits the scenarios that have  
 421 sufficient computations but need high accuracy. In Appendix D, we show an example case that could  
 422 be properly decoded with FDM but incorrectly decoded for all heuristic methods.

423 **Secondly**, in Table 3, the results reveal that FDM-A achieves an outstanding trade-off between  
 424 accuracy and speed: When we compare FDM-A’s performance with FDM, the negative influence is  
 425 marginal. The accuracy of FDM ( $K = 2$ ) on the GSM8K benchmark of the LLaDA model is 82.03%,  
 426 and for FDM-A, it achieves 81.96% (-0.07%). Meanwhile, FDM-A achieves 5.15 $\times$  speedup in TPS,  
 427 significantly improving TPS from 8.28 to 42.65. In contrast, the performance of heuristic methods  
 428 will largely degrade when their decoding step is reduced. For example, when we compare the results  
 429 in Table 2 and 3, the accuracy with the highest probability decoding declines from 81.20% to 78.17%  
 430

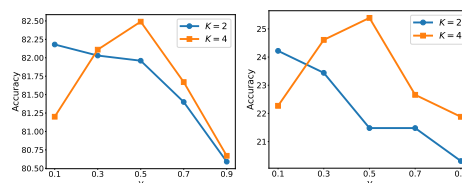
432 Table 3: Comparison (%) of FDM-A with methods that accelerate the decoding of LLDMs. The best  
 433 results are in **bold**. FDM-A achieves not only the highest accuracy, but also the fastest speed.  
 434

435 Benchmark	436 Method	437 LLaDA		438 LLaDA-1.5		439 MMaDA-MixCoT		440 LLaDA-MoE	
		441 Accuracy	442 TPS	443 Accuracy	444 TPS	445 Accuracy	446 TPS	447 Accuracy	448 TPS
449 GSM8K	Probability ( $T=128$ )	78.17	20.86	80.06	22.04	52.08	21.65	71.49	8.81
	Margin ( $T=128$ )	79.23	21.36	80.39	21.61	50.72	21.37	72.93	8.47
	Entropy ( $T=128$ )	77.94	20.69	80.22	20.71	49.13	20.51	70.66	8.39
	EB	79.61	36.46	81.35	37.74	53.83	36.39	74.53	13.98
	WINO	79.45	40.02	80.89	40.96	51.33	36.92	72.78	13.02
450 HumanEval	FDM-A (Ours)	<b>81.96</b>	<b>42.65</b>	<b>82.87</b>	<b>43.98</b>	<b>55.12</b>	<b>40.96</b>	<b>76.72</b>	<b>14.89</b>
	Probability ( $T=128$ )	35.37	16.75	39.63	17.04	7.93	16.59	51.22	7.99
	Margin ( $T=128$ )	37.20	16.25	37.20	16.58	12.80	16.15	49.39	7.74
	Entropy ( $T=128$ )	31.20	15.93	35.37	15.77	4.27	15.46	48.78	7.46
	EB	37.20	17.34	37.80	18.99	12.80	24.95	59.15	10.14
451 Countdown	WINO	39.02	18.33	40.24	20.59	12.20	29.90	56.71	9.31
	FDM-A (Ours)	<b>44.51</b>	<b>21.56</b>	<b>42.07</b>	<b>23.83</b>	<b>13.41</b>	<b>32.32</b>	<b>60.98</b>	<b>11.25</b>
	Probability ( $T=128$ )	19.53	21.19	<b>21.09</b>	22.01	12.01	21.97	44.53	8.80
	Margin ( $T=128$ )	20.31	20.65	19.92	21.76	8.59	21.57	42.58	8.33
	Entropy ( $T=128$ )	19.53	20.62	18.75	20.93	8.59	20.52	35.94	8.15
452 ARC	EB	19.20	18.68	19.92	18.79	18.75	48.51	42.19	9.48
	WINO	19.14	20.52	19.14	20.38	20.70	52.39	25.00	8.23
	FDM-A (Ours)	<b>21.48</b>	<b>21.98</b>	<b>21.09</b>	<b>22.29</b>	<b>26.95</b>	<b>62.30</b>	<b>49.61</b>	<b>10.14</b>
	Probability ( $T=128$ )	82.16	21.24	86.38	21.71	55.04	22.26	72.74	8.68
	Margin ( $T=128$ )	84.34	20.65	85.91	21.34	56.30	21.47	75.48	8.56
453	Entropy ( $T=128$ )	77.20	19.91	84.58	20.48	55.61	20.58	69.08	8.12
	EB	73.55	32.01	85.68	34.89	56.86	32.89	71.50	8.98
	WINO	79.44	34.17	85.31	35.27	56.79	34.27	70.86	7.92
	FDM-A (Ours)	<b>86.30</b>	<b>38.20</b>	<b>87.66</b>	<b>38.43</b>	<b>59.50</b>	<b>37.07</b>	<b>83.33</b>	<b>12.62</b>



(a) GSM8K

(b) Countdown



(a) GSM8K

(b) Countdown

463 Figure 4: The influence of  $K$  to model performance on GSM8K and Countdown benchmarks.  
 464

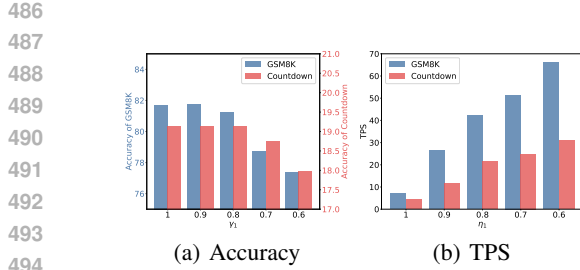
465 Figure 5: The influence of  $\gamma$  to model performance on GSM8K and Countdown benchmarks.  
 466

467 when we halve the step number. Owing to its **full** exploitation with the global confidence in the  
 468 exploration and balance stage, FDM-A also outperforms dynamic decoding methods like WINO,  
 469 demonstrating its strong capacity.

## 470 5.2 ABLATION STUDIES

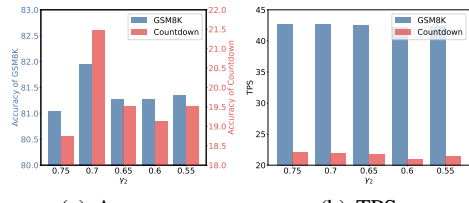
471 **Going Wider with  $K$ .** In Section 5.1, we show that larger  $K$  will benefit the performance of FDM  
 472 and a natural question is whether it will bring consistent improvement with the increase of  $K$ . Thus,  
 473 here we set  $K$  with the value from  $[2, 4, 6, 8, 10, 12]$  and perform experiments on the LLaDA model.  
 474 As summarized in both Figure 4 and Figure 8 in Appendix E, the accuracy will reach the peak  
 475 for both FDM-A and FDM. This is because although the training goal of the network is to fit the  
 476 data distribution  $p_{data}$ , in realistic, the divergence between two distributions is not zero, leading to  
 477 accumulating bias when we perform excessive searching operations, **supported by the theoretical**  
 478 **analysis in Appendix F**. Intriguingly, when we compare the curves of FDM and FDM-A, we find  
 479 that FDM outperforms FDM-A when  $K$  is larger. Conversely, FDM-A holds an advantage when  $K$   
 480 is small. This highlights the complementary role of both methods. FDM-A is suited for use when  
 481 computational resources are limited. FDM, on the other hand, provides robust capabilities under  
 482 conditions of abundant computational supply.

483 **The Setting of  $\gamma$ .** When we foresee the future impact with the global confidence, we introduce a  
 484 threshold  $\gamma$  to dynamically prune the candidate tokens of the low local confidence value. We further  
 485 investigate its effect by tuning it between 0.1 and 0.9 with  $K = 2$  and 4. Taking FDM-A as an  
 486 example, the results on LLaDA of the GSM8K and Countdown datasets are shown in Figure 5. For



(a) Accuracy

(b) TPS



(a) Accuracy

(b) TPS

Figure 6: The influence of  $\eta_1$  to Accuracy and TPS on GSM8K and Countdown benchmarks.Figure 7: The influence of  $\eta_2$  to Accuracy and TPS on GSM8K and Countdown benchmarks.

more results, please refer to Figure 9 in Appendix E. We also observe a trade-off in its configuration: the results illustrate that a smaller  $\gamma$ , e.g. 0.1, achieves better accuracy in  $K = 2$ . This is because it provides a wider choice for selection, mitigating the issue of inadequate search. However, we find that it can not maintain its advantage when  $K$  increases to 4, since more tokens of lower  $C_{local}$  are chosen, reflecting the uncertainty of models in its prediction. In contrast, if we set  $\gamma$  too large, it will suppress the exploration in the foreseeing decoding. In total,  $\gamma$  near 0.5 can balance both in its application, which is chosen as the configuration for the experiments in Section 5.1.

**The Choices of  $\eta_1$  and  $\eta_2$ .** In addition to  $K$  and  $\gamma$ , FDM-A also introduces  $\eta_1$  and  $\eta_2$  as hyperparameters for stage divisions. In the main text, we perform experiments on the GSM8K and Countdown benchmarks in Figure 6 and 7. For more results on HumanEval and ARC benchmarks, please refer to Figure 10 and 11 in Appendix E. We firstly fix  $\eta_2$  at 0.6 and linearly decrease  $\eta_1$  from 1.0 to 0.6. The results in Figure 6 (a) demonstrate that the accuracy remains stable at first, and then drops sharply in small  $\eta_1$ . In contrast, the TPS monotonically improves with the decrease of  $\eta_1$  because more tokens are parallelly decoded. By default, we set  $\eta_1$  as 0.8 because it can not only maintain the model utility but also achieve high decoding speed. Secondly, we fix  $\eta_1$  with 0.8 and set  $\eta_2$  from [0.75, 0.7, 0.65, 0.6, 0.55]. Among all configurations,  $\eta_2 = 0.7$  consistently achieves outstanding performances across all benchmarks. Because when  $\eta_2$  is large, the exploration at the balance stage is insufficient. But if  $\eta_2$  is set too small, uncertain tokens will interfere the correctness of decoding.

## 6 CONCLUSION

In this paper, we address the critical challenge of token decoding orders in Large Language Diffusion Models (LLDMs). We identify the limitations of existing heuristic methods that rely solely on local confidence, and propose a novel solution by incorporating global confidence into the decoding process. We theoretically prove that it will achieve a lower value than heuristic methods in divergence with the natural distribution. To save the computations, our proposed Foreseeing Decoding Method (FDM) optimizes decoding order through a heuristic beam search, effectively balancing local and global considerations. The accelerated variant, FDM-A, further enhances efficiency by strategically applying deep exploration only at critical steps. Extensive experiments demonstrate that FDM consistently outperforms existing baselines, serving as an effective inference-time scaling method, while FDM-A achieves an outstanding trade-off between performance and speed. Our work provides a principled approach to decoding strategy design, potentially opening new avenues for developing more powerful and efficient decoding methods for LLDMs.

## ETHICS STATEMENT

Since this work is dedicated to enhancing the efficiency and accuracy of LLDM by proposing decoding algorithms, its technical focus inherently does not involve the creation or propagation any contents of ethical issues. In addition, our research utilizes exclusively publicly available datasets and models for experiments and analysis, with all sources properly cited.

## REPRODUCIBILITY STATEMENT

The experimental settings are elaborated in detail in Section 5 and Appendix C. We will also release the source code, along with the necessary configuration files, upon acceptance.

540 REFERENCES  
541

542 Jacob Austin, Daniel D Johnson, Jonathan Ho, Daniel Tarlow, and Rianne Van Den Berg. Structured  
543 denoising diffusion models in discrete state-spaces. In *NeurIPS*, volume 34, 2021.

544 Heli Ben-Hamu, Itai Gat, Daniel Severo, Niklas Nolte, and Brian Karrer. Accelerated sampling from  
545 masked diffusion models via entropy bounded unmasking. *arXiv preprint arXiv:2505.24857*, 2025.

546 Lukas Berglund, Meg Tong, Maximilian Kaufmann, Mikita Balesni, Asa Cooper Stickland, Tomasz  
547 Korbak, and Owain Evans. The reversal curse: Llms trained on “a is b” fail to learn “b is a”. In  
548 *ICLR*, 2024.

549 Zhenni Bi, Kai Han, Chuanjian Liu, Yehui Tang, and Yunhe Wang. Forest-of-thought: Scaling  
550 test-time compute for enhancing llm reasoning. *arXiv preprint arXiv:2412.09078*, 2024.

551 Mark Chen, Jerry Tworek, Heewoo Jun, Qiming Yuan, Henrique Ponde De Oliveira Pinto, Jared  
552 Kaplan, Harri Edwards, Yuri Burda, Nicholas Joseph, Greg Brockman, et al. Evaluating large  
553 language models trained on code. *arXiv preprint arXiv:2107.03374*, 2021.

554 Peter Clark, Isaac Cowhey, Oren Etzioni, Tushar Khot, Ashish Sabharwal, Carissa Schoenick, and  
555 Oyvind Tafjord. Think you have solved question answering? try arc, the ai2 reasoning challenge.  
556 *arXiv preprint arXiv:1803.05457*, 2018.

557 Karl Cobbe, Vineet Kosaraju, Mohammad Bavarian, Mark Chen, Heewoo Jun, Lukasz Kaiser,  
558 Matthias Plappert, Jerry Tworek, Jacob Hilton, Reiichiro Nakano, et al. Training verifiers to solve  
559 math word problems. *arXiv preprint arXiv:2110.14168*, 2021.

560 Google DeepMind. Gemini diffusion, 2025. URL <https://deepmind.google/models/gemini-diffusion/>.

561 Xuanzhao Dong, Wenhui Zhu, Xiwen Chen, Zhipeng Wang, Peijie Qiu, Shao Tang, Xin Li, and  
562 Yalin Wang. Llada-medv: Exploring large language diffusion models for biomedical image  
563 understanding. *arXiv preprint arXiv:2508.01617*, 2025.

564 Guhao Feng, Yihan Geng, Jian Guan, Wei Wu, Liwei Wang, and Di He. Theoretical benefit and  
565 limitation of diffusion language model. *arXiv preprint arXiv:2502.09622*, 2025.

566 Shansan Gong, Mukai Li, Jiangtao Feng, Zhiyong Wu, and Lingpeng Kong. Diffuseq: Sequence to  
567 sequence text generation with diffusion models. In *ICLR*, 2023.

568 Shansan Gong, Shivam Agarwal, Yizhe Zhang, Jiacheng Ye, Lin Zheng, Mukai Li, Chenxin An,  
569 Peilin Zhao, Wei Bi, Jiawei Han, et al. Scaling diffusion language models via adaptation from  
570 autoregressive models. *arXiv preprint arXiv:2410.17891*, 2024.

571 Daya Guo, Dejian Yang, Haowei Zhang, Junxiao Song, Ruoyu Zhang, Runxin Xu, Qihao Zhu,  
572 Shirong Ma, Peiyi Wang, Xiao Bi, et al. Deepseek-r1: Incentivizing reasoning capability in llms  
573 via reinforcement learning. *arXiv preprint arXiv:2501.12948*, 2025.

574 Jonathan Ho, Ajay Jain, and Pieter Abbeel. Denoising diffusion probabilistic models. In *NeurIPS*,  
575 2020.

576 Feng Hong, Geng Yu, Yushi Ye, Haicheng Huang, Huangjie Zheng, Ya Zhang, Yanfeng Wang, and  
577 Jiangchao Yao. Wide-in, narrow-out: Revokable decoding for efficient and effective dllms. *arXiv  
578 preprint arXiv:2507.18578*, 2025.

579 Zhanqiu Hu, Jian Meng, Yash Akhauri, Mohamed S Abdelfattah, Jae-sun Seo, Zhiru Zhang, and  
580 Udit Gupta. Accelerating diffusion language model inference via efficient kv caching and guided  
581 diffusion. *arXiv preprint arXiv:2505.21467*, 2025.

582 inclusionAI. Llada-moe-7b-a1b-instruct, 2025. URL <https://huggingface.co/inclusionAI/LLaDA-MoE-7B-A1B-Instruct>.

583 Aaron Jaech, Adam Kalai, Adam Lerer, Adam Richardson, Ahmed El-Kishky, Aiden Low, Alec  
584 Helyar, Aleksander Madry, Alex Beutel, Alex Carney, et al. Openai o1 system card. *arXiv preprint  
585 arXiv:2412.16720*, 2024.

594 Samar Khanna, Siddhant Kharbanda, Shufan Li, Harshit Varma, Eric Wang, Sawyer Birnbaum,  
 595 Ziyang Luo, Yanis Miraoui, Akash Palrecha, Stefano Ermon, et al. Mercury: Ultra-fast language  
 596 models based on diffusion. *arXiv preprint arXiv:2506.17298*, 2025.

597

598 Jaeyeon Kim, Kulin Shah, Vasilis Kontonis, Sham M Kakade, and Sitan Chen. Train for the worst,  
 599 plan for the best: Understanding token ordering in masked diffusions. In *ICML*, 2025.

600 Gen Li and Changxiao Cai. A convergence theory for diffusion language models: An information-  
 601 theoretic perspective. *arXiv preprint arXiv:2505.21400*, 2025.

602

603 Tianyi Li, Mingda Chen, Bowei Guo, and Zhiqiang Shen. A survey on diffusion language models.  
 604 *arXiv preprint arXiv:2508.10875*, 2025.

605 Xiang Li, John Thickstun, Ishaan Gulrajani, Percy S Liang, and Tatsunori B Hashimoto. Diffusion-lm  
 606 improves controllable text generation. In *NeurIPS*, 2022.

607

608 Xinyin Ma, Runpeng Yu, Gongfan Fang, and Xinchao Wang. dkv-cache: The cache for diffusion  
 609 language models. *arXiv preprint arXiv:2505.15781*, 2025.

610 Shen Nie, Fengqi Zhu, Zebin You, Xiaolu Zhang, Jingyang Ou, Jun Hu, Jun Zhou, Yankai Lin, Ji-  
 611 Rong Wen, and Chongxuan Li. Large language diffusion models. *arXiv preprint arXiv:2502.09992*,  
 612 2025.

613

614 William Peebles and Saining Xie. Scalable diffusion models with transformers. In *Proceedings of  
 615 the IEEE/CVF international conference on computer vision*, pp. 4195–4205, 2023.

616 Fred Zhangzhi Peng, Zachary Bezemek, Sawan Patel, Jarrid Rector-Brooks, Sherwood Yao,  
 617 Avishek Joey Bose, Alexander Tong, and Pranam Chatterjee. Path planning for masked diffusion  
 618 model sampling. *arXiv preprint arXiv:2502.03540*, 2025.

619

620 Robin Rombach, Andreas Blattmann, Dominik Lorenz, Patrick Esser, and Björn Ommer. High-  
 621 resolution image synthesis with latent diffusion models. In *CVPR*, 2022a.

622

623 Robin Rombach, Andreas Blattmann, Dominik Lorenz, Patrick Esser, and Björn Ommer. High-  
 624 resolution image synthesis with latent diffusion models. In *Proceedings of the IEEE/CVF confer-  
 625 ence on computer vision and pattern recognition*, pp. 10684–10695, 2022b.

626

627 Charlie Snell, Jaehoon Lee, Kelvin Xu, and Aviral Kumar. Scaling lilm test-time compute optimally  
 628 can be more effective than scaling model parameters. *arXiv preprint arXiv:2408.03314*, 2024.

629

630 Kimi Team, Yifan Bai, Yiping Bao, Guanduo Chen, Jiahao Chen, Ningxin Chen, Ruijue Chen, Yanru  
 631 Chen, Yuankun Chen, Yutian Chen, et al. Kimi k2: Open agentic intelligence. *arXiv preprint  
 632 arXiv:2507.20534*, 2025.

633

634 Chengyue Wu, Hao Zhang, Shuchen Xue, Zhijian Liu, Shizhe Diao, Ligeng Zhu, Ping Luo, Song  
 635 Han, and Enze Xie. Fast-dllm: Training-free acceleration of diffusion lilm by enabling kv cache  
 636 and parallel decoding. *arXiv preprint arXiv:2505.22618*, 2025.

637

638 Zhihui Xie, Jiacheng Ye, Lin Zheng, Jiahui Gao, Jingwei Dong, Zirui Wu, Xueliang Zhao, Shansan  
 639 Gong, Xin Jiang, Zhenguo Li, et al. Dream-coder 7b: An open diffusion language model for code.  
 640 *arXiv preprint arXiv:2509.01142*, 2025.

641

642 Zhen Xiong, Yujun Cai, Zhecheng Li, and Yiwei Wang. Unveiling the potential of diffusion large  
 643 language model in controllable generation. *arXiv preprint arXiv:2507.04504*, 2025.

644

645 Ling Yang, Ye Tian, Bowen Li, Xinchen Zhang, Ke Shen, Yunhai Tong, and Mengdi Wang. Mmada:  
 646 Multimodal large diffusion language models. *arXiv preprint arXiv:2505.15809*, 2025.

647

648 Jiacheng Ye, Zhihui Xie, Lin Zheng, Jiahui Gao, Zirui Wu, Xin Jiang, Zhenguo Li, and Lingpeng  
 649 Kong. Dream 7b: Diffusion large language models. *arXiv preprint arXiv:2508.15487*, 2025.

650

651 Zebin You, Shen Nie, Xiaolu Zhang, Jun Hu, Jun Zhou, Zhiwu Lu, Ji-Rong Wen, and Chongxuan  
 652 Li. Llada-v: Large language diffusion models with visual instruction tuning. *arXiv preprint  
 653 arXiv:2505.16933*, 2025.

648 Siyan Zhao, Devaansh Gupta, Qinqing Zheng, and Aditya Grover. d1: Scaling reasoning in diffusion  
649 large language models via reinforcement learning. *arXiv preprint arXiv:2504.12216*, 2025.  
650

651 Lin Zheng, Jianbo Yuan, Lei Yu, and Lingpeng Kong. A reparameterized discrete diffusion model for  
652 text generation. In *COLM*, 2024.

653 Fengqi Zhu, Rongzhen Wang, Shen Nie, Xiaolu Zhang, Chunwei Wu, Jun Hu, Jun Zhou, Jianfei  
654 Chen, Yankai Lin, Ji-Rong Wen, et al. Llada 1.5: Variance-reduced preference optimization for  
655 large language diffusion models. *arXiv preprint arXiv:2505.19223*, 2025.  
656

657

658

659

660

661

662

663

664

665

666

667

668

669

670

671

672

673

674

675

676

677

678

679

680

681

682

683

684

685

686

687

688

689

690

691

692

693

694

695

696

697

698

699

700

701

702 **A USAGE OF LLM**  
 703

704 In this paper, we employ Large Language Models (LLMs) to polish writing and assist in debugging.  
 705 All LLM-polished text is rechecked by the authors to ensure accuracy and prevent over-claims or  
 706 confusions.  
 707

708 **B PROOF OF THEOREM 1**  
 709

710 Define the single-step KL errors  
 711

$$\varepsilon_t^H \triangleq D_{KL}(p_{data}(\mathbf{x}_t | \mathbf{x}_{t-1}), \pi_H(\mathbf{x}_t)), \quad \varepsilon_t^F \triangleq D_{KL}(p_{data}(\mathbf{x}_t | \mathbf{x}_{t-1}), \pi_F(\mathbf{x}_t)).$$

712 We first prove that  
 713

$$\varepsilon_t^F = \varepsilon_t^H - \mathcal{I}_{p_{data}}(\mathbf{x}_t; \mathbf{x}_T | \mathbf{x}_{t-1}), \quad (19)$$

714 where  $\mathcal{I}_{p_{data}}(\mathbf{x}_t; \mathbf{x}_T | \mathbf{x}_{t-1})$  is the conditional mutual information under  $q$ . Since  $\mathbf{x}_{t-1}$  and  $\mathbf{q}$  can be  
 715 considered as fixed variables at the step  $t$ , we omit them in the notation for brevity. According to the  
 716 definition of KL divergence, we have:  
 717

$$\varepsilon_t^F \triangleq D_{KL}(p_{data}(\mathbf{x}_t), \pi_F(\mathbf{x}_t)) = \sum_{\mathbf{x}_t} p_{data}(\mathbf{x}_t) [\log p_{data}(\mathbf{x}_t) - \log \pi_F(\mathbf{x}_t)]. \quad (20)$$

718 By construction  
 719

$$\pi_F(\mathbf{x}_t) = \frac{\exp(S(\mathbf{x}_t))}{Z_t}, \quad S(\mathbf{x}_t) = C_{\text{local}}(\mathbf{x}_t) + C_{\text{global}}(\mathbf{x}_t), \quad Z_t = \sum_{\mathbf{x}'_t} \exp(S(\mathbf{x}'_t)).$$

720 Hence  
 721

$$\log \pi_F(\mathbf{x}_t) = S(\mathbf{x}_t) - \log Z_t = C_{\text{local}}(\mathbf{x}_t) + C_{\text{global}}(\mathbf{x}_t) - \log Z_t. \quad (21)$$

722 By inserting Equation 21 into 20 and split the sum,  
 723

$$\begin{aligned} \varepsilon_t^F &= \sum_{\mathbf{x}_t} p_{data}(\mathbf{x}_t) [\log p_{data}(\mathbf{x}_t) - C_{\text{local}}(\mathbf{x}_t) - C_{\text{global}}(\mathbf{x}_t) + \log Z_t] \\ &= \underbrace{\sum_{\mathbf{x}_t} p_{data}(\mathbf{x}_t) [\log p_{data}(\mathbf{x}_t) - C_{\text{local}}(\mathbf{x}_t)]}_{\text{Term A}} - \underbrace{\sum_{\mathbf{x}_t} p_{data}(\mathbf{x}_t) [C_{\text{global}}(\mathbf{x}_t) - \log Z_t]}_{\text{Term B}}. \end{aligned} \quad (22)$$

724 By definition  $C_{\text{local}}(\mathbf{x}_t) = \log p_{\theta}(\mathbf{x}_t)$ , so  
 725

$$\text{Term A} = \sum_{\mathbf{x}_t} p_{data}(\mathbf{x}_t) [\log p_{data}(\mathbf{x}_t) - \log p_{\theta}(\mathbf{x}_t)] = D_{KL}(p_{data}(\mathbf{x}_t), p_{\theta}(\mathbf{x}_t)) \triangleq \varepsilon_t^H. \quad (23)$$

726 First recall  
 727

$$C_{\text{global}}(\mathbf{x}_t) = \mathbb{E}_{x' \sim p_{\theta}} \log p_{\theta}(x' | \mathbf{x}_t) = \sum_{\mathbf{x}_T} p_{\theta}(\mathbf{x}_T | \mathbf{x}_t) \log p_{\theta}(\mathbf{x}_T | \mathbf{x}_t).$$

728 Therefore  
 729

$$\begin{aligned} \text{Term B} &= \sum_{\mathbf{x}_t} p_{data}(\mathbf{x}_t) [C_{\text{global}}(\mathbf{x}_t) - \log Z_t] \\ &= \sum_{\mathbf{x}_t} p_{data}(\mathbf{x}_t) \left[ \sum_{\mathbf{x}_T} p_{\theta}(\mathbf{x}_T | \mathbf{x}_t) \log p_{\theta}(\mathbf{x}_T | \mathbf{x}_t) - \log Z_t \right]. \end{aligned} \quad (24)$$

730 Next we use the identity  $Z_t = p_{\theta}(\mathbf{x}_T)$  (marginal over  $\mathbf{x}'_t$ ), which follows from  
 731

$$Z_t = \sum_{\mathbf{x}'_t} \exp(S(\mathbf{x}'_t)) = \sum_{\mathbf{x}'_t} p_{\theta}(\mathbf{x}'_t, \mathbf{x}_T) = p_{\theta}(\mathbf{x}_T).$$

732 Hence  
 733

$$\log Z_t = \log p_{\theta}(\mathbf{x}_T) = \sum_{\mathbf{x}_T} p_{\theta}(\mathbf{x}_T | \mathbf{x}_t) \log p_{\theta}(\mathbf{x}_T),$$

where the second equality holds because  $p_\theta(\mathbf{x}_T)$  does not depend on  $\mathbf{x}_t$  and  $\sum_{\mathbf{x}_t} p_\theta(\mathbf{x}_T \mid \mathbf{x}_t) = 1$ . Inserting this into Equation 24 gives

$$\begin{aligned}
\text{Term B} &= \sum_{\mathbf{x}_t} p_{data}(\mathbf{x}_t) \sum_{\mathbf{x}_T} p_{\theta}(\mathbf{x}_T \mid \mathbf{x}_t) \left[ \log p_{\theta}(\mathbf{x}_T \mid \mathbf{x}_t) - \log p_{\theta}(\mathbf{x}_T) \right] \\
&= \sum_{\mathbf{x}_t, \mathbf{x}_T} p_{data}(\mathbf{x}_t, \mathbf{x}_T) \left[ \log \frac{p_{\theta}(\mathbf{x}_T \mid \mathbf{x}_t)}{p_{\theta}(\mathbf{x}_T)} \right] \\
&= \sum_{\mathbf{x}_t, \mathbf{x}_T} p_{data}(\mathbf{x}_t, \mathbf{x}_T) \left[ \log \frac{p_{data}(\mathbf{x}_t, \mathbf{x}_T)}{p_{data}(\mathbf{x}_t)p_{data}(\mathbf{x}_T)} \right] \quad (\text{replace } p_{\theta} \text{ with } q \text{ inside log}) \\
&= \mathcal{I}_{p_{data}}(\mathbf{x}_t; \mathbf{x}_T). \tag{25}
\end{aligned}$$

Inserting Equation 23 and 25 into Equation 22 yields

$$\varepsilon_t^F = \varepsilon_t^H - \mathcal{I}_{p_{data}}(\mathbf{x}_t; \mathbf{x}_T).$$

which completes the proof of Equation 19. Using the chain rule for KL divergence over sequences we have

$$D_{KL}(p_{data}(\mathbf{x}), p_{\pi_F}) = \sum_{t=1}^T \mathbb{E}_{p_{data}(\mathbf{x}_{t-1})} [\varepsilon_t^F] = \sum_{t=1}^T \mathbb{E}_{p_{data}(\mathbf{x}_{t-1})} [\varepsilon_t^H - \mathcal{I}_{p_{data}}(\mathbf{x}_t; \mathbf{x}_T | \mathbf{x}_{t-1})].$$

## Recognising the definitions

$$\sum_{t=1}^T \mathbb{E}_{p_{data}(\mathbf{x}_{t-1})} \varepsilon_t^H = D_{KL}(p_{data}(\mathbf{x}), p_{\pi_H}), \quad \sum_{t=1}^T \mathbb{E}_{p_{data}(\mathbf{x}_{t-1})} \mathcal{I}_{p_{data}}(\mathbf{x}_t; \mathbf{x}_T | \mathbf{x}_{t-1}) = \Delta_{\text{total}},$$

we obtain

$$D_{KL}(p_{data}(\mathbf{x}), p_{\pi_F}) = D_{KL}(p_{data}(\mathbf{x}), p_{\pi_H}) - \Delta_{\text{total}},$$

which finishes the proof of Theorem 1.

## C SYSTEM PROMPTS FOR EVALUATION

## GSM8K

You are a math expert. You will be given a question to solve. Solve it step by step. Wrap the final answer in a `\boxed{ }` .

Respond in the following format:

<reasoning>

Your reasoning here

</reasoning >

<answer>

\boxed{...}

</answer>

ARC

You will be given a multiple choice question and a list of options. You need to first reason step by step, and then select the correct option (A, B, C, D). Wrap the single letter of the correct option in `\boxed{...}`. Respond in the following format:

### <reasoning>

Your reasoning here

</reasoning>

<answer>

\boxed{..}

810

811

**Countdown**

812

813

814

815

816

817

Using only the provided numbers, create an arithmetic expression that evaluates to exactly the provided target number. You may use the operations  $+$ ,  $-$ ,  $*$ , and  $/$  as needed, but each number must be used exactly once. Think step-by-step. After reasoning, provide only your final expression inside  $\boxed{\quad}$  tags without including an equals sign or the target number. For example:  $\boxed{a + b * c}$

Respond in the following format:

<reasoning>

Your reasoning here

</reasoning>

<answer>

$\boxed{\dots}$

</answer>

823

824

825

**HumanEval**

Write a solution to the following problem and make sure that it passes the tests:

python

831

**D THE EXAMPLE CASE**

834

835

**Question in the ARC benchmark**

836

837

Which of the following is the primary way that evergreen trees planted on the north and west sides of residences in Massachusetts help reduce winter heating costs?

838

A They insulate against cold air

839

B They optimize solar heating.

840

C They reduce radiant cooling.

841

D They act as a windbreak.

842

843

844

**Decoding with the highest probability (Incorrect)**

845

846

847

848

Evergreen trees planted on the north and west sides of residences in Massachusetts help reduce winter heating costs primarily by acting as a physical barrier against cold air. This trees' asymmetrical and dense foliage provide a natural insulation, preventing cold air from entering the home, thereby reducing the need for heating.

</reasoning>

<answer>

$\boxed{A}$

</answer>

853

854

855

**Decoding with the highest margin (Incorrect)**

856

857

858

859

Evergreen trees planted on the north and west sides of residences in Massachusetts can help reduce winter heating costs by providing as much solar heat as possible. This is because the trees can capture and store sunlight, which can be used to heat the home during the winter months. By maximizing the amount of solar heat, the trees can help reduce the need for additional heating systems.

</reasoning>

<answer>

B

864

**Decoding with the lowest entropy (Incorrect)**

865

Evergreen trees are planted on the north and west sides of residences in Massachusetts to help reduce winter heating costs. The primary reason for this benefit is due to the insulation provided by the trees. The trees provide insulation against the cold, reducing the amount of heat escaping the house and keeping the interior temperature slightly warmer. This insulation reduces the need for heating, thereby making the home more efficient.

866

&lt;/answer&gt;

867

\boxed{A}

868

869

870

871

872

873

874

875

**Decoding with FDM (Correct)**

876

Evergreen trees planted on the north and west sides of residences in Massachusetts can help reduce winter heating costs by acting as a windbreak. These trees can block cold air from entering the home, reducing the need for heating. Additionally, evergreen trees can also provide insulation against cold air, but the primary benefit is their role as a windbreak.

877

&lt;/reasoning&gt;

878

&lt;/answer&gt;

879

\boxed{D}

880

881

882

883

884

885

886

**E ABLATION STUDIES ON THE HUMAN EVAL AND ARC BENCHMARKS**

887

We perform experiments on the HumanEval and ARC benchmarks with the experimental settings in Section 5.2. We observe that the optimal hyperparameter has good transferability across datasets.

888

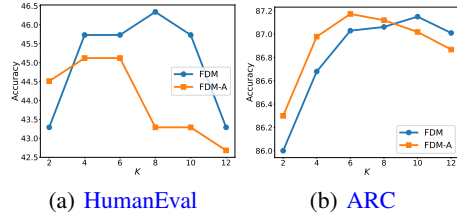
889

890

891

892

893



(a) HumanEval

(b) ARC

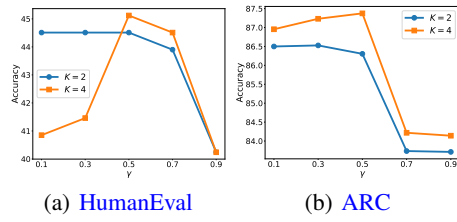
894

895

896

897

898



(a) HumanEval

(b) ARC

899

900

901

902

903

904

905

906

907

908

909

910

911

912

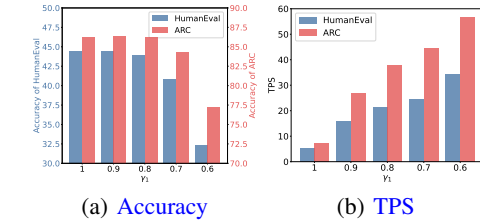
913

914

915

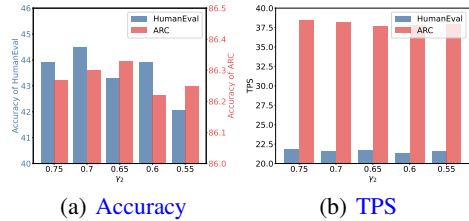
916

917

Figure 8: The influence of  $K$  to model performance on HumanEval and ARC benchmarks.Figure 10: The influence of  $\eta_1$  to Accuracy and TPS on HumanEval and ARC benchmarks.

(a) Accuracy

(b) TPS

Figure 9: The influence of  $\gamma$  to model performance on HumanEval and ARC benchmarks.Figure 11: The influence of  $\eta_2$  to Accuracy and TPS on HumanEval and ARC benchmarks.

(a) Accuracy

(b) TPS

918 **F THEORETICAL ANALYSIS FOR PERFORMANCE DEGRADATION WITH A  
919 EXTREMELY LARGE  $K$**

921 We next present a theoretical analysis to support that the degradation in performance is due to the  
922 consequence of noise-amplified selection in the mismatch between the model and natural distributions.  
923 At each decoding step, we have  $K$  candidate tokens whose true future returns are  
924

$$925 \quad s_1, \dots, s_K \in \mathbb{R}, \quad s_* = \max_i s_i, \text{ where } s_i \triangleq \log p_{\text{data}}(\mathbf{x}_t = \text{i-th candidate token} \mid \mathbf{x}_{t-1}, \mathbf{q}).$$

927 When  $K$  is large enough, we can assume that the token with the highest possibility in the real data  
928 distribution is already in the candidates. The model in our algorithm only observes confidence scores,  
929 which are noisy estimates of true future returns:

$$930 \quad \hat{s}_i = s_i + \xi_i$$

931 Here we hypothesize that  $\xi_i$  is independent and identically distributed (i.i.d.) Gaussian random  
932 variables:  
933

$$\xi_i \stackrel{\text{iid}}{\sim} \mathcal{N}(0, \sigma^2)$$

935 and  $\hat{s}_i$  is equal to the sum of the local and global confidence of the i-th candidate token:  
936

$$937 \quad \hat{s}_i = C_{\text{local}}(\text{i-th candidate token}) + C_{\text{global}}(\text{i-th candidate token})$$

938 According to Equation 8, our algorithm selects the candidate with the highest  $\hat{s}_i$ :

$$939 \quad j = \arg \max_{i \in [K]} \hat{s}_i.$$

941 For any sub-optimal candidate  $i$  with confidence gap  $\Delta_i = s_* - s_i > 0$ , the probability that noise  
942 flips the ranking is  
943

$$944 \quad \Pr(\hat{s}_i > \hat{s}_*) = \Pr(\xi_i - \xi_* > \Delta_i) = \Phi\left(-\frac{\Delta_i}{\sqrt{2}\sigma}\right),$$

946 where  $\Phi(\cdot)$  is the standard normal tail CDF(Cumulative Distribution Function). Union-bounding over  
947 the  $K - 1$  sub-optimal candidates yields  
948

$$949 \quad \Pr(\text{select non-optimal}) \leq \sum_{i \neq *} \Phi\left(-\frac{\Delta_i}{\sqrt{2}\sigma}\right).$$

951 The RHS(right hand side) increases monotonically with  $K$  whenever there exist  $\Delta_i = O(\sigma)$ . On the  
952 other hand, let  $\xi_{(K)} = \max_{i \leq K} \xi_i$ . The Extreme-value Theory gives  
953

$$954 \quad \mathbb{E}[\xi_{(K)}] \approx \sigma \sqrt{2 \ln K}.$$

955 Hence, the selected estimate satisfies  
956

$$957 \quad \mathbb{E}[\hat{s}_j] \approx s_* + \sigma \sqrt{2 \ln K},$$

958 while the true return of the selected candidate satisfies:  
959

$$960 \quad \mathbb{E}[s_j] \leq s_* + \underbrace{\mathbb{E}[\xi_{(K)} - \xi_j]}_{\geq 0}.$$

963 Consequently, the expected regret is:  
964

$$965 \quad \mathbb{E}[\Delta_j] = \mathbb{E}[s_* - s_j] \geq C\sigma \sqrt{\ln K}$$

966 which grows with  $K$ , providing a quantitative lower bound for the “winner’s curse” in the decoding  
967 process. Because each incorrect selection changes the subsequent context, the regret accumulates  
968 along the generation process. Early mistakes (where  $K$  is too large in our schedule) therefore have a  
969 negative effect, explaining the empirical observation in Figure 4 and 8.  
970  
971